Manipulating the radiation pattern of equilateral triangular dielectric resonator antenna using asymmetric grooves

Manipulating the Radiation Pattern of Equilateral Triangular Dielectric Resonator Antenna Using Asymmetric Grooves

Saeed Fakhte[1*], Sumer Singh Singhwal[2], Ladislau Matekovits[2,3,4], and Binod Kumar Kanaujia[5]

[1] School of Electrical and Computer Engineering, Qom University of Technology, Qom, Iran

[2] Department of Electronics and Telecommunications, Politecnico di Torino, Turin, Italy

[3] Instituto di Elettronica e di Ingegneria dell'Informazione e delle Telecomunicazioni, National Research Council of Italy, Turin, Italy

[4] Department of Measurements and Optical Electronics, Politehnica University Timisoara, Romania.

[5] School of Computational and Integrative Sciences, Jawaharlal Nehru University, New Delhi, India.

* Corresponding Author: fakhte@qut.ac.ir

***Abstract*—** A new method to manipulate the radiation pattern of a triangular dielectric resonator antenna is proposed here. By engraving asymmetric grooves in the antenna walls, the intensity of electric fields on its walls is adjusted, which, if properly done, leads to an increase in the directivity of the antenna. Then, the possibility of rotating the radiation pattern by creating asymmetric grooves in the antenna wall is investigated. It is proved that by adjusting the ratio of the amplitude of equivalent magnetic currents on the antenna walls, rotation can be created in the main beam of the antenna pattern. The simulation results are validated by measuring the reflection coefficient, radiation patterns, and gain of the DRA. The measured results confirm that the antenna operates from 3.1 to 3.8 GHz and the maximum gain is 9.2 dBi.

Keywords—radiation pattern, impedance bandwidth, gain, dielectric resonator antenna (DRA).

1. INTRODUCTION

Dielectric resonator antennas (DRA) have been of great interest to researchers in recent years due to their unique features., such as broad impedance bandwidth, compact structure, and low losses [1-6]. So far, various methods have been reported in the literature to increase the gain of the DRAs [7-13]. One of the methods that has been introduced in recent years by some of the authors of the present work consists of increasing the radiation from the sidewalls of the antenna [10]. It is proved that by adjusting the ratio of the amplitude of the equivalent magnetic currents on the antenna walls, a more directive pattern can be achieved. This method has been applied to rectangular DRA with symmetrical grooves in the antenna walls [10] as well as using anisotropic materials [11]. Moreover, the method demonstrates its functionality in cylindrical [12] and

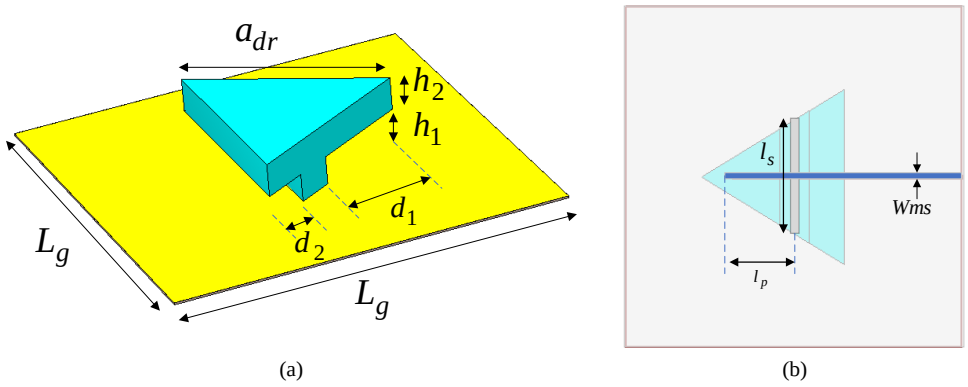

Figure 1. The structure of proposed DRA. (a) Three-dimensional view, (b) Top view (In the rendering, a transparent dielectric has been used to make visible the feeding slot and the ground plane).

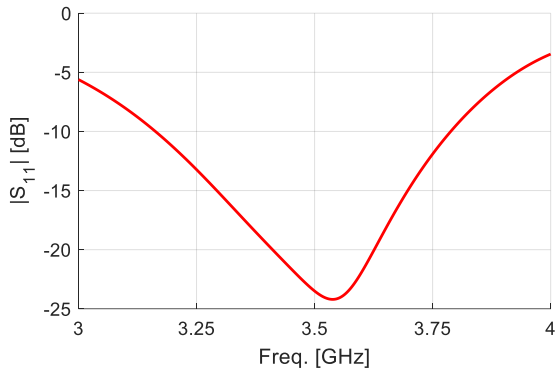

Figure 2. Simulated $|S_{11}|$ of the proposed antenna.

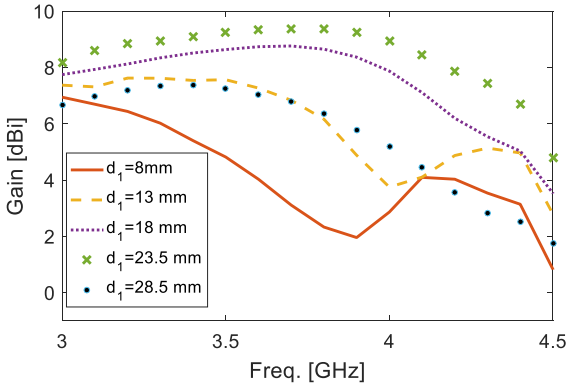

Figure 3. The variation of antenna gains for different values of the engraving depth. The antenna parameters are as follows: $d_2 = 10.7$, $h_1 = 7.1$, $h_2 = 8.3$, $a_{dr} = 50$, $l_g = 100$, $l_s = 23.3$, $l_p = 18.3$, $w_{ms} = 1.15$ mm.

triangular DRAs [13] in combination with the use of anisotropic materials. In [13], using an anisotropic material in the triangular DRA, a peak gain of 8.1 dBi is obtained, which is higher with 2 dB that can be obtained neglecting the anisotropic material.

In the present work, by engraving asymmetric grooves in the walls of the triangular DRA, a maximum gain of 9.2 dBi has been achieved, which is approximately 1.1 dBi more than the gain reported in [13]. The asymmetric configuration has not been previously reported for the use of

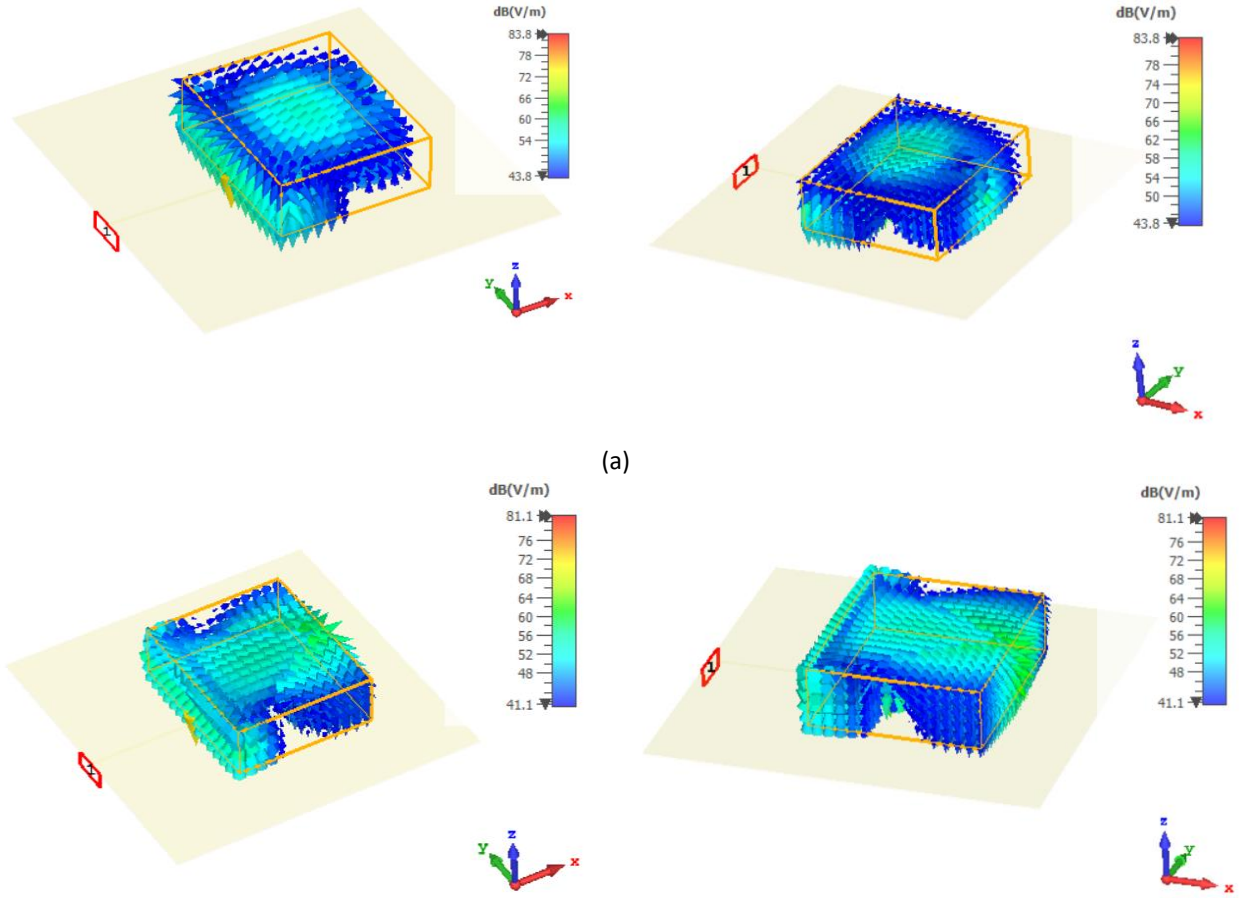

Figure 4. Electric field distribution of the TM_{101}^{z} mode of the TDRA obtained from simulation for antennas with (a) symmetric engraving at 2.8 GHz and (b) asymmetric engraving at 3.5 GHz.

gain enhancement in any geometry of DRAs, hence it represents the main novelty of this work. In fact, due to the particular geometry of the triangular DRA, it is proven that engraving asymmetric grooves leads to a higher gain than symmetrical ones. Although the innovation of this work consists of the use of asymmetric grooves to enhance the gain of the antenna, even the use of symmetrical grooves for this purpose has not been reported so far. On the other hand, compared to the rectangular antenna reported in [10], even though this antenna achieves a gain of 9.6 dBi by engraving symmetrical grooves on its walls, but the triangular antenna occupies a lower surface area, which is the advantage of triangular antennas compared to the rectangular and cylindrical structures [14]. Also, another innovation of this work is the study of rotation of the main beam of the antenna radiation pattern by manipulating the currents on the side walls. Examining the available literature, one can see that the use of asymmetric grooves in the antenna walls to rotate the main beam of the antenna has not been reported so far. Finally, due to the introduction of air regions inside the antenna structure, one can see that the antenna bandwidth has also increased.

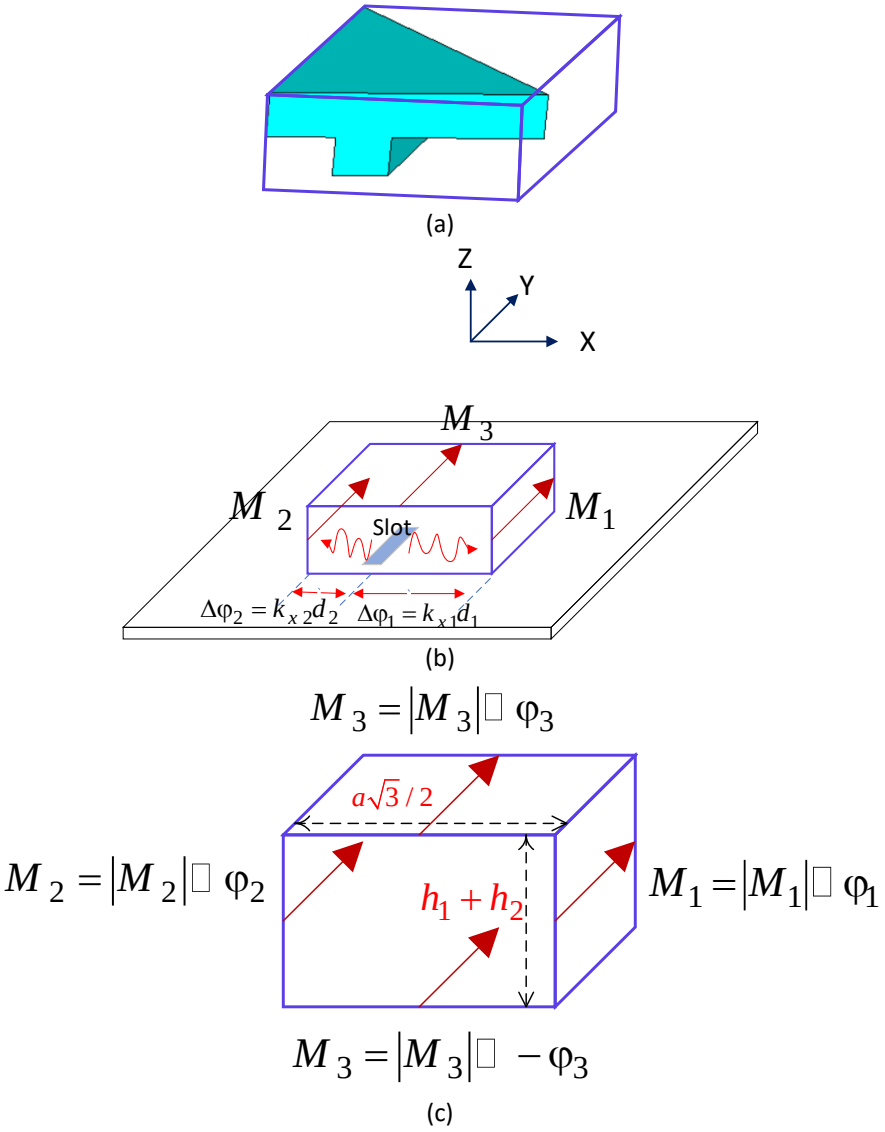

Figure 5. Modeling of the DRA with magnetic current densities on the hypothetical box surface surrounding the triangle. (a) Antenna with surrounding box, (b) Radiation model of the antenna on the ground plane, (c) Box extension with relative surface magnetic current densities after applying the image and equivalence theorems.

The paper is structured as follows: in section II, the geometry of the proposed antenna is described and an approximate method for obtaining the antenna resonant frequency is explained. Then the superiority of using asymmetric grooves instead of symmetrical ones is demonstrated in an approximate theoretical way. Finally, in section III, the experimental results are presented.

2. Antenna Configuration

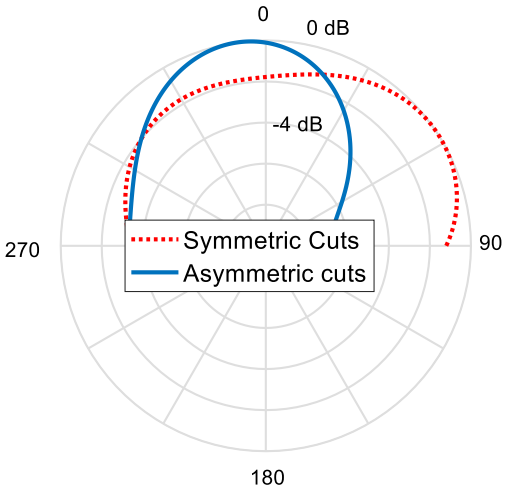

Figure 6. The E-plane radiation patterns obtained from the theoretical method.

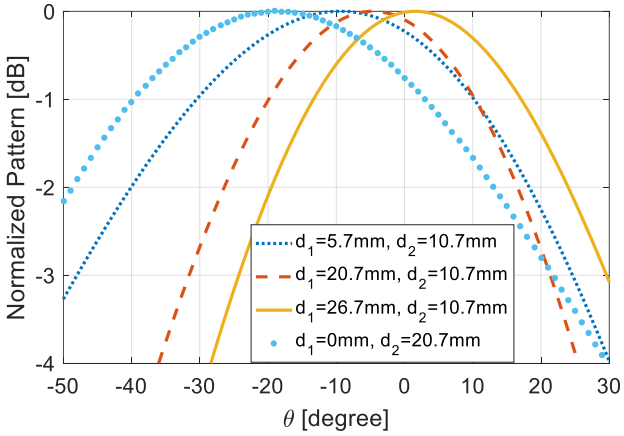

Figure 7. The proposed antenna simulated radiation pattern for different values of engraving depths. The values of the other parameters are the same as before.

Fig. 1 displays the proposed structure. As displayed, the triangular DRA is fed using a slot in the ground plane. The DRA is made of Eccostock Hik with $\varepsilon_r = 10$ and loss tangent of 0.001. The slot is also fed using a microstrip line placed on the other side of the RO 4003 substrate. The DRA parameters reported in Fig. 1 are as follows: a_{dr} , d_1, d_2 , h_1, h_2 . The antenna lays on a ground plane of extension of $L_g \times L_g$. Also, the lengths of the slot and the open-end stub are l_s and l_p , respectively. As shown in the figure, grooves with the heights of h_1 and depths of d_1 and d_2 are created on the right and left sides of the initial triangular prism, respectively.

The proposed antenna is optimized with the aim of achieving the best results in terms of bandwidth and gain, and the value of the optimized parameters are as follows: $d_1 = 23.5$, $d_2 = 10.7$, $h_1 = 7.1$, $h_2 = 8.3$, $a_{dr} = 50$, $l_g = 100$, $l_s = 23.3$, $l_p = 18.3$, $w_{ms} = 1.15$ mm.

The excited mode in the TDRA is TM^{z}_{101} mode, so to obtain an initial guess of the antenna dimensions, the resonant frequency formula of this mode can be used [15].

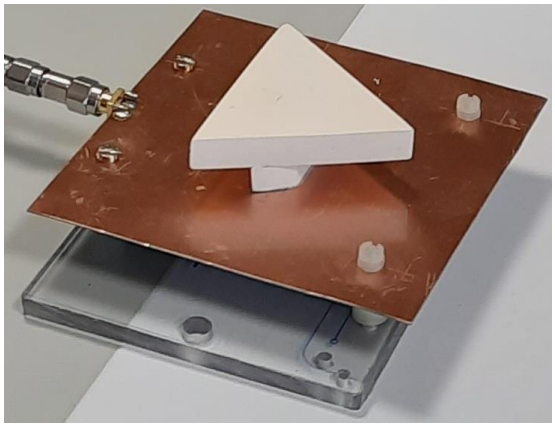

Figure 8. Photograph of the antenna fabricated prototype.

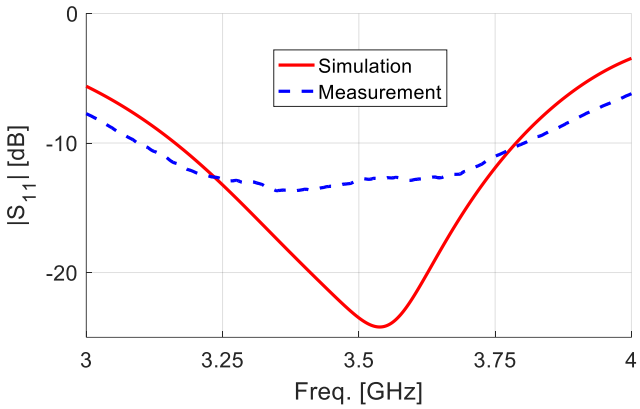

Figure 9. The measured and simulated reflection coefficient of the proposed antenna.

$$f_r = \frac{c}{2\pi\sqrt{\varepsilon_{eff}}}\sqrt{\chi^2 + k_z^2} \tag{1}$$

where c is the speed of light, $\chi = \frac{4\pi}{3a_{eff}}$, $k_z = \frac{\pi}{2d_{eff}}$, ε_{eff} is the effective dielectric constants of the dielectric and air regions inside the triangular prism, a_{eff} and d_{eff} are the effective length and height of the prism. These effective parameters are obtained using the following formulas [15, 16]:

$$\varepsilon_{eff} = \frac{\varepsilon_r \times V_{dielectric} + 1 \times V_{air}}{V_{dielectric} + V_{air}} \tag{2}$$

$$a_e = a_{dr} \times \left(1.003 \times e^{-0.0001747} - 0.4172 \times e^{-0.4967}\right) - 0.01 \times \left(\frac{h_1 + h_2}{a_{dr}}\right) \times \varepsilon_{eff}^{-1.75}; \tag{3}$$

$$d_e = (h_1 + h_2) \times \left(1 - 1.0 \times \varepsilon_{eff}^{-1}\right) \tag{4}$$

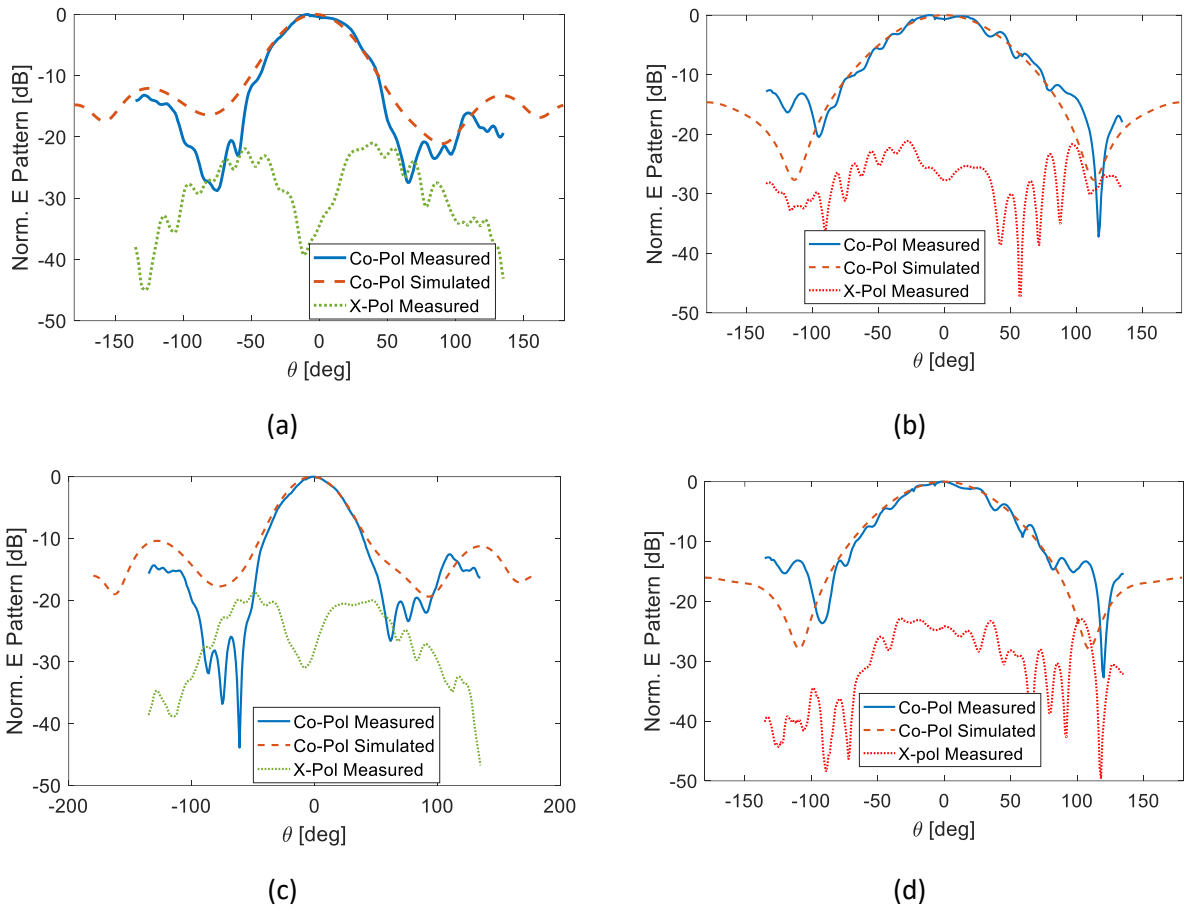

Figure 10. Simulated and measured radiation patterns of the proposed antenna in (a) XoZ plane at 3.5 GHz, (b) YoZ plane at 3.5 GHz, (c) XoZ plane at 3.75 GHz, (d) YoZ plane at 3.75 GHz.

All geometrical parameters are as displayed in Fig. 1. Using this method, the resonant frequency of the proposed antenna with the final optimized dimensions mentioned above is calculated to be 3 GHz.

The design method is as follows: to increase the antenna directivity in the $\boldsymbol{\theta = 0}$ direction, it is assumed from the geometric shape of the triangular DRA that the engraving depth 1 should be greater than the engraving depth 2. Therefore, as an initial guess, the engraving depths 1 and 2 are considered to be 0.4 and 0.2 of the side lengths of the triangle, respectively, i.e., $\boldsymbol{d_1 = 0.4a_{dr}}$and $\boldsymbol{d_2 = 0.2a_{dr}}$. Also, the thickness of the engravings is considered to be half the height of the DRA, i.e., $\boldsymbol{h_1 = h_2 = 0.5h_{dr}}$. Note that these assumptions are approximate.

In the following, using formula (2), we calculate the effective dielectric coefficient of the TDRA:

$$\varepsilon_{eff} = \frac{\varepsilon_r \times V_{dielectric} + 1 \times V_{air}}{V_{dielectric} + V_{air}} \tag{5}$$

$$V_{dielectric} = \frac{\sqrt{3}}{2} a_{dr}^2 h_1 - h_1 \left(\frac{d_1^2}{\sqrt{3}} + a d_2 - \frac{d_2^2}{\sqrt{3}}\right) \tag{6}$$

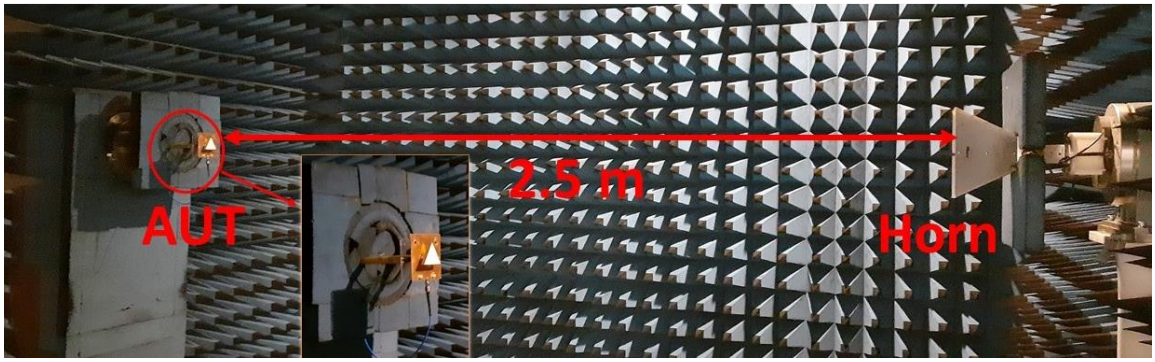

Figure 11. Antenna gain measurement setup in the anechoic chamber.

$$V_{air} = h_1\left(\frac{d_1^2}{\sqrt{3}} + ad_2 - \frac{d_2^2}{\sqrt{3}}\right) \quad (7)$$

$$V_{dielectric} + V_{air} = \frac{\sqrt{3}}{2} a_{dr}^2 h_1 \quad (8)$$

Then, by placing this effective dielectric coefficient along with the effective length and height of TDRA from equations (3) and (4), in equation (1), the TDRA resonant frequency is obtained. After obtaining the initial dimensions using this design method, in the next step, we optimize the structure using parametric study in CST.

The simulated result of the antenna reflection coefficient is drawn in Fig. 2. Note that the resonant frequency value obtained from the theoretical method is approximately close to the value obtained from the simulation and it can be used to obtain an initial guess of the antenna dimensions. However, due to the complexity of the antenna structure, this discrepancy between the results of the theoretical method and the simulation is acceptable.

Fig. 3 shows the variations of the antenna gain for different values of the engraving depth on the right side of the prism, d_1. It can be seen that the best gain is achieved when the engraving depths on the right and left sides of the antenna are not equal, i.e $d_1 \neq d_2$. To justify this, the electric field distributions for two antennas with symmetric and asymmetric grooves are plotted in Fig. 4. Since the antennas with asymmetric ($d_1 = 23.5$ mm, $d_2 = 10.7$ mm) and symmetrical grooves ($d_1 = 10.7$ mm, $d_2 = 10.7$ mm) operate at 3.5 and 2.8 GHz, respectively, their electric field distributions are shown at these two frequencies. As displayed in the figure, the electric field distributions are plotted inside a hypothetical rectangular box around the triangular antenna. Fig. 4a shows the distribution of the electric field in the antenna with symmetrical grooves in two different perspective views. Observe that the intensity of the electric field on the left side of the box is stronger than that of the right side. But in Fig. 4b, where the electric field distribution is plotted for the antenna with asymmetric grooves, one can see that the electric field intensities on the left and right sides of the box are almost equal. As shown in Fig. 5, according to the equivalence principle, to obtain the far-field radiation pattern of the antenna, the far-field radiation of the equivalent current densities on the surface of this hypothetical box can be calculated. This model has been used to calculate the DRA

far-field radiation pattern in many references [1], [10], [12]. In fact, in this model, it is assumed that the DRA is located on a large ground plane and the effect of the ground plane is eliminated by doubling the height of the DRA and using the image theorem [1]. Considering the complex structure of TDRA, this model has been only used to describe the behavior of the far-field radiation pattern of the antenna. Only the magnetic current densities in the y direction are considered on the box surfaces, because it can be proved that the radiated fields due to the electric current densities are much weaker than those of the magnetic current densities [10]. Also, because the slot distance from the box walls is different, the equivalent magnetic current densities on the walls have different phases relative to each other. Fig. 5b shows that the effective wavenumber $\boldsymbol{k_x}$ for the wave entering the dielectric from the slot takes different values depending on whether it moves in the direction of the x-axis (positive) or the opposite direction. This is due to the geometry of the dielectric part, which has more volume on one side than the other. In Fig. 5c, the phase of each magnetic current density is indicated next to it. Note that this model, although not computationally accurate, can be used to qualitatively justify the antenna radiation behavior. Finally, by using the image theorem, the following approximate relation can be obtained to calculate the far-field electric field of the antenna.

$$\begin{aligned} &E(\theta,\varphi) = E(\textit{magnetic dipole}) \times \\ &(M_3 e^{jk_0 \cos\theta \frac{(h_1+h_2)}{2}} + M_3 e^{-jk_0 \cos\theta \frac{(h_1+h_2)}{2}} \\ &+ M_1 e^{-jk_0 \sin\theta \cos\varphi \frac{a\sqrt{3}}{4}} + M_2 e^{jk_0 \sin\theta \cos\varphi \frac{a\sqrt{3}}{4}}) \end{aligned} \tag{5}$$

$$\bar{M} = \hat{n} \times \bar{E} = \begin{cases} E_z \hat{y}, \textit{left} \\ E_x \hat{y}, \textit{top} \\ -E_z \hat{y}, \textit{right} \\ -E_x \hat{y}, \textit{bottom} \end{cases} \tag{6}$$

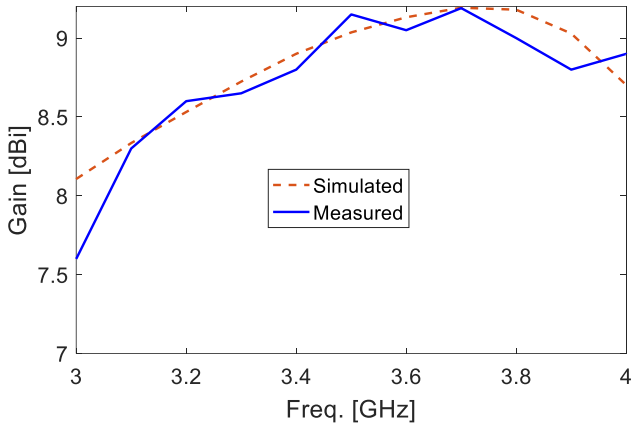

Figure 12. Simulated and measured gain of the proposed antenna.

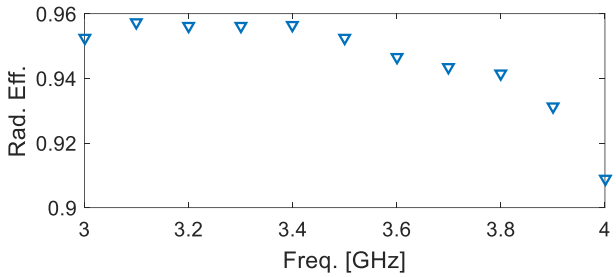

Figure 13. Simulated radiation efficiency of the proposed antenna.

where $\hat{n}$ is the unit vector normal to the walls of the box, M1, M2 and M3 are the magnetic current densities on the walls of the rectangular cube and k_0 is the wavenumber of free space.

In order to give a rough estimate of the ratio of magnetic current densities on the box walls, the ratio of the amplitude of the electric fields in the middle of the different walls and the phase differences between them are obtained using simulation. The following results are obtained: $|M_2|/|M_1|=1.7$, $\angle\varphi_2-\angle\varphi_1=-224°$ and $|M_3|/|M_1|=1.28$, $\angle\varphi_3-\angle\varphi_1=-234°$ for the case with symmetrical grooves and $|M_2|/|M_1|=1$, $\angle\varphi_2-\angle\varphi_1=-343°$ and $|M_3|/|M_1|=0.76$, $\angle\varphi_3-\angle\varphi_1=-358°$ for the case with asymmetric grooves. By inserting these results in Eq. (5), the normalized far-field radiation patterns of both antennas are calculated, as shown in Fig. 6. Each curve is normalized to its maximum value. Observe that for the proposed optimized antenna with asymmetric grooves, the main beam of the radiation pattern is towards θ= 0, but for the antenna with symmetrical grooves, the main beam of the radiation pattern is rotated by an angle of 60° relative to the z-axis. This is why the gain is higher in the structure with asymmetric grooves than in the structure with symmetrical grooves. As a result, by using engravings with different depths in DRA, the main beam direction of the antenna radiation pattern can be changed.

The simulated radiation patterns of the DRA for different values of engraving depths, d_1, d_2, are plotted in Fig. 7. Note that by changing the parameters d1 and d2, the antenna resonant frequency changes, and the patterns drawn in Fig. 7 are obtained at their corresponding resonant frequencies. It can be seen that by decreasing the engraving depth d_1 compared to the engraving depth d_2, the

direction of the main beam of the radiation pattern deviates from the angle $\theta = 0^o$ and rotates to the left by an angle of 20^o. As the difference between these two parameters, i.e. $d_2 - d_1$, increases, the rotation of the main beam increases. In fact, by changing the parameters d1 and d2, the amplitude of the electric fields and, consequently, the amplitude of the equivalent magnetic current densities on the walls change. It can be seen from Equation (5) that if the amplitudes and phases of M1, M2 and M3 change relative to each other, the rotation of the pattern can be created. For applications in which we need an antenna with the main beam direction to an angle other than zero degrees, this technique can be used to rotate the main beam direction of the radiation pattern.

3. Results and Discussion

A prototype of the triangular DRA with asymmetric grooves has been fabricated. A little glue was used on the bottom edge of the TDRA to fix the TDRA to the ground. Then it is pressed in a mechanical clamp and left for a few hours until the glue dries. However, by this process, a little air may be trapped between the layers and is expected to have little effect on response. In this prototype, the antenna has the highest boresight gain. A photograph of the fabricated prototype is displayed in Fig. 8. The measured result of the reflection coefficient is shown in Fig. 9. Reasonable agreement between the simulation and measurement is attained, with the discrepancy mainly caused by the errors in the fabrication of the complex structure of the TDRA. Anyway, this amount of discrepancy between the fabrication and simulation results in the literature of the DRA antenna is acceptable and it has been reported in many articles [17, 18, 19, and 20]. The proposed DRA operates from 3.1 to 3.8 GHz, which covers the WiMAX frequency band. Fig. 10 shows the measured and simulated radiation patterns of the proposed directive antenna at the frequencies of 3.5 GHz and 3.75 GHz. Observe that the maximum antenna gain is obtained in the direction of $\theta = 0$. Also, a broadside radiation pattern is observed in both XoZ and YoZ planes. The discrepancy between the results at the angles outside the half-power beamwidth range of the antenna is due to measurement and fabrication errors. The ripples in the measured patterns are due to the diffraction from the antenna mount in the anechoic chamber. The test setup used to measure the antenna gain is shown in Fig. 11. As shown, a reference horn antenna is placed in front of the proposed antenna at a distance of 2.5 meters, and the power transmitted by the horn antenna is received and measured by the proposed antenna. From the difference between the power received by the proposed antenna and the power transmitted by the reference horn antenna, the boresight gain is calculated. Fig.12 shows the simulation and experimental results of the gain of the proposed antenna. Observe that the maximum gain of 9.2 dBi is achieved at 3.6 GHz. Also, the radiation efficiency above 90% is achieved over the whole operation band, as shown in Fig. 13.

4. Conclusion

A new technique has been introduced to increase the directivity of the triangular dielectric resonator antenna operating at the fundamental mode. This method is based on increasing the

radiation from the side walls of the antenna compared to the upper wall. To achieve this, asymmetric grooves on both sides of the triangular prism have been engraved. Also, by using an approximate theoretical method, it is seen that by using asymmetric grooves, the direction of the main beam of the antenna radiation pattern can be rotated. The experimental results of the DRA are provided to confirm the performance of the proposed antenna.

References

1. A. Petosa, *Dielectric Resonator Antenna Handbook*, Norwood, MA, Artech House, 2007.
2. W. M. Abdel Wahab, D. Busuioc, and S. Safavi-Naeini, “Low-cost planar waveguide technology-based dielectric resonator antenna (DRA) for millimeter-wave applications: Analysis, design, and fabrication,” *IEEE Transactions on Antennas and Propagation*, vol. 58, no. 8, pp. 2499– 2507, Aug 2010.
3. S. Fakhte, H. Oraizi and R. Karimian, "A Novel Low-Cost Circularly Polarized Rotated Stacked Dielectric Resonator Antenna," in *IEEE Antennas and Wireless Propagation Letters*, vol. 13, no. , pp. 722-725, 2014.
4. Chih-Yu Huang, Jian-Yi Wu, and Kin-Lu Wong, “Cross-slot-coupled microstrip antenna and dielectric resonator antenna for circular polarization,” *IEEE Transactions on Antennas and Propagation*, vol. 47, no. 4, pp. 605–609, April 1999.
5. Q. Rao, T. A. Denidni, and A. R. Sebak, “Broadband compact stacked T-shaped dra with equilateral-triangle cross sections,” *IEEE Microwave and Wireless Components Letters*, vol. 16, no. 1, pp. 7–9, Jan 2006.
6. M. Abedian, S. K. A. Rahim, and M. Khalily, “Two-segments compact dielectric resonator antenna for UWB application,” *IEEE Antennas and Wireless Propagation Letters*, vol. 11, pp. 1533–1536, 2012.
7. E. Baldazzi *et al*., "A High-Gain Dielectric Resonator Antenna With Plastic-Based Conical Horn for Millimeter-Wave Applications," in *IEEE Antennas and Wireless Propagation Letters*, vol. 19, no. 6, pp. 949-953, June 2020.
8. A. Petosa and S. Thirakoune, “Rectangular dielectric resonator antennas with enhanced gain,” *IEEE Trans. Antennas Propag.*, vol. 59, no. 4, pp. 1385–1389, Apr. 2011.
9. Z. Chen *et al*., "Millimeter-Wave Rectangular Dielectric Resonator Antenna Array With Enlarged DRA Dimensions, Wideband Capability, and High-Gain Performance," in *IEEE Transactions on Antennas and Propagation*, vol. 68, no. 4, pp. 3271-3276, April 2020.
10. S. Fakhte, H. Oraizi and L. Matekovits, "Gain Improvement of Rectangular Dielectric Resonator Antenna by Engraving Grooves on Its Side Walls," in *IEEE Antennas and Wireless Propagation Letters*, vol. 16, pp. 2167-2170, 2017.
11. S. Fakhte, H. Oraizi and L. Matekovits, "High Gain Rectangular Dielectric Resonator Antenna Using Uniaxial Material at Fundamental Mode," in *IEEE Transactions on Antennas and Propagation*, vol. 65, no. 1, pp. 342-347, Jan. 2017.

12. S. Fakhte, H. Oraizi, L. Matekovits and G. Dassano, "Cylindrical Anisotropic Dielectric Resonator Antenna with Improved Gain," in *IEEE Transactions on Antennas and Propagation*, vol. 65, no. 3, pp. 1404-1409, March 2017.
13. S. Fakhte, I. Aryanian and L. Matekovits, "Analysis and Experiment of Equilateral Triangular Uniaxial-Anisotropic Dielectric Resonator Antennas," in *IEEE Access*, vol. 6, pp. 63071-63079, 2018.
14. K. W. Leung, K. M. Chow and K. M. Luk, "Low-profile high-permittivity dielectric resonator antenna excited by a disk-loaded coaxial aperture," in *IEEE Antennas and Wireless Propagation Letters*, vol. 2, pp. 212-214, 2003.
15. S. Maity and B. Gupta, ‘‘Theoretical investigations on equilateral triangular dielectric resonator antenna,’’ *IET Microw., Antennas Propag.*, vol. 11, no. 2, pp. 184–192, 2017.
16. S. Fakhte, H. Oraizi and R. Karimian, "A Novel Low-Cost Circularly Polarized Rotated Stacked Dielectric Resonator Antenna," in *IEEE Antennas and Wireless Propagation Letters*, vol. 13, pp. 722-725, 2014.
17. E. Baldazzi *et al*., "A High-Gain Dielectric Resonator Antenna with Plastic-Based Conical Horn for Millimeter-Wave Applications," in *IEEE Antennas and Wireless Propagation Letters*, vol. 19, no. 6, pp. 949-953, June 2020.
18. M. Yang, Y. Pan, Y. Sun and K. Leung, "Wideband Circularly Polarized Substrate-Integrated Embedded Dielectric Resonator Antenna for Millimeter-Wave Applications," in *IEEE Transactions on Antennas and Propagation*, vol. 68, no. 2, pp. 1145-1150, Feb. 2020.
19. A. Motevasselian, A. Ellgardt and B. L. G. Jonsson, "A Circularly Polarized Cylindrical Dielectric Resonator Antenna Using a Helical Exciter," in IEEE Transactions on Antennas and Propagation, vol. 61, no. 3, pp. 1439-1443, March 2013.
20. Z. Zhao, J. Ren, Y. Liu, Z. Zhou and Y. Yin, "Wideband Dual-Feed, Dual-Sense Circularly Polarized Dielectric Resonator Antenna," in IEEE Transactions on Antennas and Propagation, vol. 68, no. 12, pp. 7785-7793, Dec. 2020.